

Article

TiO₂/LaFeO₃ Composites for the Efficient Degradation of Benzoic Acid and Hydrogen Production

Isabella Natali Sora ^{1,*} , Benedetta Bertolotti ¹, Renato Pelosato ¹ , Andrea Lucotti ² , Matteo Tommasini ²  and Marica Muscetta ³ 

¹ Dipartimento di Ingegneria e Scienze Applicate, Università di Bergamo, Viale Marconi 5, 24044 Dalmine, Italy; benedetta.bertolotti@unibg.it (B.B.); renato.pelosato@unibg.it (R.P.)

² Dipartimento di Chimica, Materiali e Ingegneria Chimica “G. Natta”, Politecnico di Milano, Piazza Leonardo da Vinci 32, 20133 Milano, Italy; andrea.lucotti@polimi.it (A.L.); matteo.tommasini@polimi.it (M.T.)

³ Dipartimento di Ingegneria Chimica, dei Materiali e della Produzione (DICMaPI), Università di Napoli Federico II, Piazzale V. Tecchio 80, 80125 Naples, Italy; marica.muscetta@unina.it

* Correspondence: isabella.natali-sora@unibg.it

Abstract: LaFeO₃/TiO₂ composites were prepared in the range 0–12.2 wt% of LaFeO₃, characterized, and tested for both benzoic acid (BA) and 4-methoxycinnamic acid (MCA) degradation in aqueous solution, and hydrogen evolution. The preparation method was via ball-milling without thermal treatment. The composite materials presented agglomerates of LaFeO₃ with an average size from 1 to 5 µm, and the TiO₂ powder was well dispersed onto the surface of each sample. They showed varying activities for BA degradation depending on composition and light wavelength. The 6.2 wt% and 12.2 wt%-LaFeO₃/TiO₂ composites exhibited the highest activity under 380–800 nm light and could degrade BA in 300 min at BA concentration 13.4 mg L^{−1} and catalyst 0.12 g L^{−1}. Using a 450 nm LED light source, all composites degraded less than 10% of BA, but in the presence of H₂O₂ (1 mM) the photocatalytic activity was as high as 96% in <120 min, 6.2 wt%-LaFeO₃/TiO₂ composite being the most efficient sample. It was found that in the presence of H₂O₂, BA degradation followed first order kinetic with a reaction rate constant of 4.8 × 10^{−4} s^{−1}. The hydrogen production rate followed a classical volcano-like behavior, with the highest reactivity (1600 µmol h^{−1} g^{−1} at 60 °C) in the presence of 3.86%wt- LaFeO₃/TiO₂. It was also found that LaFeO₃/TiO₂ exhibited high stability in four recycled tests without losing activity for hydrogen production. Furthermore, a discussion on photogenerated charge-carrier transfer mechanism is briefly provided, focusing on lacking significant photocatalytic activity under 450 nm light, so p-n heterojunction formation is unlikely.

Keywords: lanthanum ferrite; benzoic acid degradation; photocatalytic hydrogen evolution; semiconductor photocatalyst



Academic Editors: Lin Huang and Yinghuai Zhu

Received: 14 March 2025

Revised: 26 March 2025

Accepted: 27 March 2025

Published: 29 March 2025

Citation: Natali Sora, I.; Bertolotti, B.; Pelosato, R.; Lucotti, A.; Tommasini, M.; Muscetta, M. TiO₂/LaFeO₃ Composites for the Efficient Degradation of Benzoic Acid and Hydrogen Production. *Molecules* **2025**, *30*, 1526. <https://doi.org/10.3390/molecules30071526>

Copyright: © 2025 by the authors. Licensee MDPI, Basel, Switzerland. This article is an open access article distributed under the terms and conditions of the Creative Commons Attribution (CC BY) license (<https://creativecommons.org/licenses/by/4.0/>).

1. Introduction

Many semiconductor oxides can act as photocatalysts [1–5]. Their activation occurs by irradiation with photons of energy that match the band gap energy of the semiconductor, resulting in electron excitation from the valence band (VB) to the conduction band (CB), thereby generating holes in the VB. Due to band bending, the photogenerated e^- - h^+ pairs diffuse to the semiconductor surface where, in the absence of electron and hole scavengers, their recombination takes place in a few nanoseconds. Recombination is avoided if an adequate scavenger or surface defect states are available to trap electron-hole pairs. In this case, water adsorbed or hydroxyl groups present on the semiconductor surface can

be oxidized by h^+ , generating HO^\bullet ($H_2O + h^+ \rightarrow HO^\bullet + H^+$), while adsorbed $O_{2\ ads}$ can be reduced by e^- , generating superoxide radicals $O_2^{\bullet-}$ ($O_{2\ ads} + e^- \rightarrow O_2^{\bullet-}$) [6]. The photocatalytic processes exploit the produced radicals to start a chemical reaction or to increase the reaction rate.

The broad utilization of semiconductor photocatalysts for organic pollutant decomposition in wastewater treatment plants has been limited by the high recombination of the photogenerated electron–hole pairs, resulting in low quantum efficiency of photocatalyzed reactions. Titanium dioxide (TiO_2) is one of the most employed materials among photocatalysts [7,8]. It shows high activity when exposed to light and excellent chemical stability. Anatase TiO_2 has an indirect and relatively large bandgap of $E_g = 3.2$ eV; for activation it requires the use of UV light which is more expensive and dangerous than radiation in the visible range [9]. Because of these challenges, nanocomposite catalysts in which one component consists of anatase TiO_2 have been extensively studied with two main objectives: to improve the separation of photogenerated electron and hole pairs, and to obtain a TiO_2 -based photocatalyst also active under visible light irradiation.

In recent years, different types of materials (e.g., ceramic, metallic, carbon-based, and polymeric nanomaterials) have been combined with TiO_2 to form functional nanocomposites, exhibiting attractive chemical and physical properties as compared to any of the components separately. $LaFeO_3$ is a stable and non-toxic semiconductor with a p-type low band gap of 2.4–2.5 eV [10]. The use of $LaFeO_3$ in photocatalytic degradation of persistent organic pollutants in wastewater, i.e., pharmaceuticals, has been previously investigated by us [11–13].

Although there are studies showing the visible-light photocatalytic degradation of (i) dyes by $LaFeO_3/TiO_2$ nanocomposite [14] and anatase- TiO_2 /rutile- $TiO_2/LaFeO_3$ three-phase nanostructured heterojunctions [15]; (ii) phenol by $LaFeO_3/TiO_2$ nanocomposite [16]; (iii) antibiotics by $LaFeO_3/TiO_2$ heterostructures [17] and by carbon quantum dot modified $TiO_2@LaFeO_3$ hollow core shell [18]; and (iv) pesticides by $LaFeO_3/TiO_2$ heterojunction [19] and core shell [20], as far as we know the photocatalytic degradation of aromatic carboxylic acids such as benzoic acid using $LaFeO_3/TiO_2$ has never been reported previously. Hydrothermal or wet chemical synthesis are the most common strategies for the preparation of these composites [14,16].

This study is focused on the photocatalytic performance of $LaFeO_3/TiO_2$ nanocomposites, (with 0–12.2 wt% of $LaFeO_3$) prepared via a fast and simple ball-milling method without thermal treatment. Benzoic acid (BA) was chosen as a model compound suitable for investigating the photocatalytic behavior of aromatic acids in an aqueous environment. The photocatalytic activity was evaluated for the degradation of BA by UV-vis spectrophotometry and high-pressure liquid chromatography (HPLC). The photocatalytic activity of the composites was evaluated with and without hydrogen peroxide addition. Presently, H_2 is mainly produced by steam methane reforming, which involves the use of fossil fuels and high temperature, resulting in low-purity hydrogen products and greenhouse gas emissions. Alternative more sustainable processes to produce high-purity H_2 are via electrochemical and photochemical water splitting [21,22]. For better evaluation of the nanocomposites, the photocatalytic hydrogen production rate using methanol as a sacrificial agent was studied. The photocatalytic hydrogen evolution performance of $LaFeO_3/TiO_2$ has been the subject of a few investigations. Lv et al. [23] synthesized 20 wt%- $LaFeO_3/TiO_2$ nanocomposites by a 2-step approach and reported that they exhibited a H_2 production rate of $0.279\text{ mmol h}^{-1}\text{ g}^{-1}$ under the simulated solar light irradiation of a 300 W Xe lamp (320–780 nm). Comparison of photocatalytic water splitting H_2 evolution rate of 20 wt%- $LaFeO_3/TiO_2$ without using methanol as a sacrificial agent gives $0.0178\text{ mmol h}^{-1}\text{ g}^{-1}$ and no hydrogen generation was observed in the presence of bare TiO_2 or $LaFeO_3$. Recently,

a 49.64 wt%-LaFeO₃/TiO₂ powder was prepared by Jiang et al. [24] via solid state method, annealing the mixture at 500 °C for 12 h in Ar atmosphere. The powder showed a high photocatalytic H₂ production rate of ~3.26 mmol h^{−1} g^{−1} under AM 1.5 simulated sunlight, which is approximately 2.28 times that of commercial TiO₂ P25 (1.43 mmol h^{−1} g^{−1}).

2. Results and Discussion

2.1. Phase Composition and Microstructure

As shown from X-ray diffraction (XRD) data, the LaFeO₃ powder (sample F) is monophasic, and the diffraction peaks can be indexed with orthorhombic ABO₃-type perovskite structure (JCPDS file No. 37-1493). The broad peaks suggest that obtained products have nanometric size. The XRD patterns of the composites B (1.3 wt%-LaFeO₃/TiO₂), C (3.9 wt%-LaFeO₃/TiO₂), D (6.2 wt%-LaFeO₃/TiO₂) and E (12.2 wt%-LaFeO₃/TiO₂) are presented in Figure 1a. Diffraction peaks belonging to the LaFeO₃, TiO₂ anatase (JCPDS card no. 21-1272), and TiO₂ rutile (JCPDS card no. 21-1276) phases were detected in all composites. By increasing the LaFeO₃ content (i.e., from B to E), the intensity of the orthoferrite diffraction peaks increases. No reaction products were observed in the XRD patterns of the composites. The XRD patterns confirm that the composites are physical mixtures of the two components as expected due to the short milling time. SEM micrographs of C, D and E composites are shown in Figure 1b–d. For brevity, other micrographs of the samples are shown in the Supporting Information (Figures S1 and S2). As shown in Figure S1, LaFeO₃ powder is nanometric, very porous, and tends to agglomerate to larger particles, causing fast charge recombination. In the SEM micrographs of C, D and E, the same microstructure is evidenced: the agglomerates of LaFeO₃ have an average size in the 1 to 5 μm range and the TiO₂ powder is well dispersed onto the surface of each sample. This characteristic may have some relationship with their good performance on the photocatalytic degradation of benzoic acid.

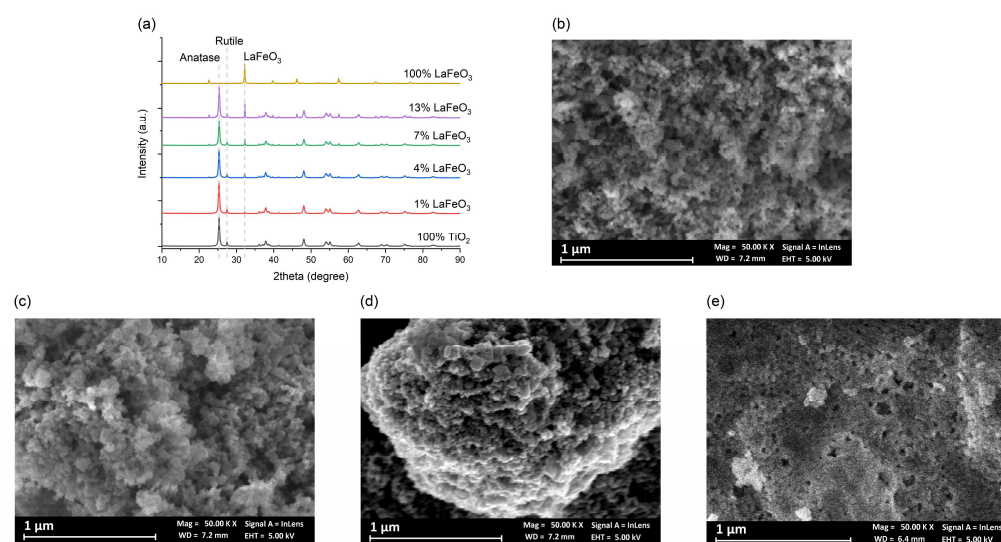


Figure 1. (a) XRD patterns of B-D-E nanocomposites and the reference compounds TiO₂ and LaFeO₃; (b) SEM image of C; (c) SEM image of D; (d) SEM image of E; (e) SEM image of LaFeO₃.

To investigate the optical absorption characteristics of LaFeO₃, nanoparticles at different wavelengths diffuse reflectance spectroscopy (DRS) analytical techniques were used. The UV–vis DRS spectrum (Figure S3) of LaFeO₃ nanoparticles shows the absorption edge occurs at about 600 nm, attributed to its electron transitions from valence band (mainly mixed *e_g* states of Fe 3*d* and O 2*p*) to conduction band (*t_{2g}* states of Fe 3*d*) [25]. A broad

absorption band ranging from 200 to 600 nm indicates its potential applications as visible light-driven photocatalyst. LaFeO₃ optical band-gap energy was 2.47 eV.

2.2. Benzoic Acid Degradation Using Daylight Lamps in LaFeO₃/TiO₂ Water Suspensions

Figure 2 shows the variation of the concentration of BA during the reactions over different catalysts, without an oxidizing agent such as H₂O₂, under visible light and a fraction of UV-A (380–800 nm). According to HPLC data, the LaFeO₃/TiO₂ composites degrade up to 93% of BA in 300 min. Pure TiO₂ (sample A) and LaFeO₃ (sample F) degraded 80% and 9% in 300 min, respectively. In Table 1 these results are compared with those of other LaFeO₃/TiO₂ photocatalysts on organic pollutant degradation using UV or visible light. The experimental studies are performed with a catalyst concentration in the range 0.8–2.4 g L^{−1}, larger than the one used in this study (0.12 g L^{−1}).

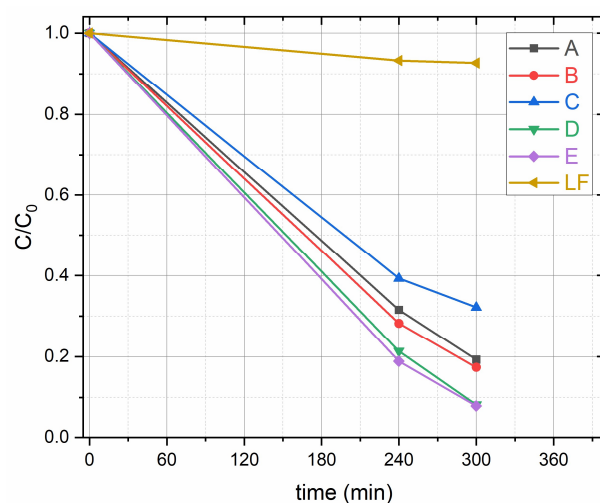


Figure 2. Photocatalytic degradation of BA in the presence of samples A (TiO₂), B (1.3 wt%-LaFeO₃/TiO₂), C (3.9 wt%-LaFeO₃/TiO₂), D (6.2 wt%-LaFeO₃/TiO₂), E (12.2 wt%-LaFeO₃/TiO₂) and LF (LaFeO₃) from HPLC analysis. Experimental conditions: 0.120 g L^{−1} catalyst loading, [BA] = 1 × 10^{−4} M, λ = 380–800 nm light.

TiO₂ powder covers LaFeO₃ agglomerates, so it is likely that the BA adsorption on composites is similar to that of TiO₂. BA adsorption depends on the surface charge of TiO₂ and on the extent of BA deprotonation ($K_a = 6.46 \times 10^{-5}$ at 25 °C). The TiO₂ surface is positively charged at pH below the point of zero charge at $\text{pH}_{\text{zpc}} \approx 6$ [26]. At natural pH, $\text{pH} \approx 4.2$ – 4.6 in A to E suspensions, BA adsorption should be favored through electrostatic interactions between the negatively charged benzoate ion $\text{C}_6\text{H}_5\text{COO}^-$ in the water matrix and the $-\text{OH}_2^+$ groups on the TiO₂ surface. In suspension F, pH is ≈ 6.1 , and the benzoate would be attracted to the most positively charged LaFeO₃ surface ($\text{pH}_{\text{zpc}} = 8.9$) through electrostatic interactions. It seems that no direct relationship can be established between the pH_{zpc} values and the photoactivity of the samples. However, given the good performance of the D and E composites in the degradation of BA, it could be assumed that BA is more easily degraded under a relatively weak acidic pH_{zpc} value, since it is a weak acid.

Another factor that could influence photocatalytic activity is the surface area of the catalysts. Perovskite oxides usually have small surface areas and large particle sizes. In particular, sample F (LaFeO₃) presents a specific surface area of 14 m² g^{−1} significantly smaller than that of bare TiO₂ (48 m² g^{−1}), which is detrimental to the number of the available surface-active sites. Since the effective separation of the photogenerated e^- - h^+ pairs are a key aspect in photocatalytic reactions, the large particle size of LaFeO₃ can have some relationship with a difficult migration of electrons or holes onto the surface of

LaFeO₃ to react with adsorbed BA rather than to recombine with each other. According to the mechanism described above, it is not difficult to understand that TiO₂-containing composites show a higher photocatalytic activity compared to pure LaFeO₃.

Table 1. Pollutant photodegradation over LaFeO₃/TiO₂ composites.

Photocatalyst	LaFeO ₃ :TiO ₂	Radiation	Organic Compound	Catalyst	Removal (%)	Time (min)	Ref.
LaFeO ₃ /TiO ₂ rutile calcination 800 °C/6 h	1.5:1 (m/m)	visible	methyl orange	n.a.	90	180	[14]
LaFeO ₃ @TiO ₂ heterojunction	5:100	300–800 nm	myclobutanil 20 mg L ^{−1}	1 g L ^{−1}	100	180	[19]
LaFeO ₃ @TiO ₂ heterojunction	12.5:100	>420 nm	myclobutanil 20 mg L ^{−1}	1 g L ^{−1}	37	240	[19]
LaFeO ₃ /TiO ₂ anatase calcination 500 °C/3 h	3:100	>420 nm	ciprofloxacin 10 mg L ^{−1}	2.4 g L ^{−1}	100	90	[17]
LaFeO ₃ /TiO ₂ (P25) calcination 450 °C/2 h	0.85:100	254 nm	thiamethozam 20 mg L ^{−1}	0.8 g L ^{−1}	97	120	[20]
LaFeO ₃ /TiO ₂ (P25) calcination 450 °C/2 h	0.85:100	direct sunlight	thiamethozam 20 mg L ^{−1}	0.8 g L ^{−1}	79	120	[20]
LaFeO ₃ /TiO ₂ (P25) ball-milling	6.2:100	LED450 nm	benzoic acid 13.4 mg L ^{−1}	0.12 g L ^{−1} H ₂ O ₂ 1 mM	96	120	this work
LaFeO ₃ /TiO ₂ (P25) ball-milling	6.2:100	LED 450 nm	benzoic acid 13.4 mg L ^{−1}	0.12 g L ^{−1}	9	120	this work
LaFeO ₃ /TiO ₂ (P25) ball-milling	6.2:100	380–800 nm	benzoic acid 13.4 mg L ^{−1}	0.12 g L ^{−1}	90	300	this work

As reported in previous studies [27] (Ajmera et al., 2002 [28]), the photocatalytic degradation of BA proceeds through HO• radical attack preferentially on the *ortho* and *para* positions, producing hydroxy-benzoic acids and dihydroxy-benzoic acids, according to HPLC analysis. The intermediate species go through photocatalytic degradation in competition with BA, slowing down the BA degradation. As shown in Figure 3, a second hydroxylation and subsequent ring opening is likely to follow but the species expected to evolve from here would be small molecule organics (i.e., methanol) that would rapidly degrade to carbon dioxide.

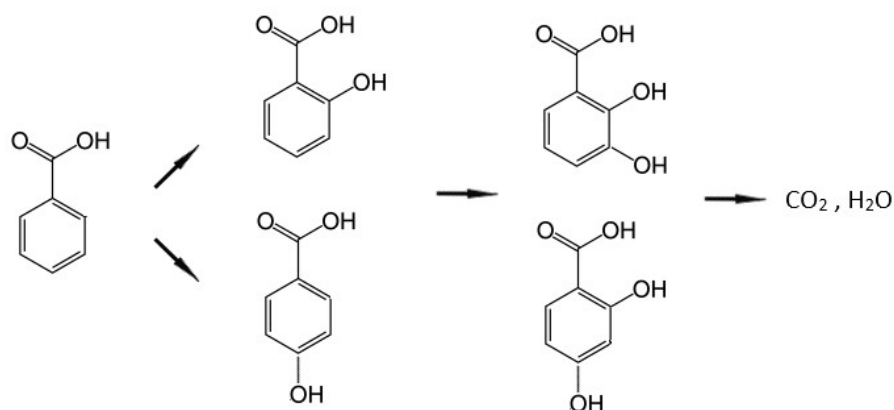


Figure 3. Pathway of degradation of benzoic acid following ref. [28].

The decrease of benzoic acid and the formation of salicylic acid after one hour of irradiation was assessed qualitatively using fluorescence spectroscopy. Figure 4 illustrates the temporal changes in the emission spectra of benzoic acid in aqueous solutions irradiated for one hour in the presence of a fixed amount of the photocatalysts A (Figure 4a), E (Figure 4b), and F (Figure 4c). Under identical conditions, benzoic acid emits significantly less than salicylic acid [29]. The small emission peak of benzoic acid at approximately 300 nm decreases after one hour of irradiation in the solutions prepared with A and E but not the one prepared with F. This is consistent with the HPLC data shown in Figure 2. For the photocatalysts A and E, after one hour of illumination, a new emission band appears at about 410 nm, which is a typical feature of salicylic acid excited at a wavelength of 230 nm [29]. Therefore, it is clear that salicylic acid is one of the intermediates produced during the degradation of benzoic acid by OH radical attack.

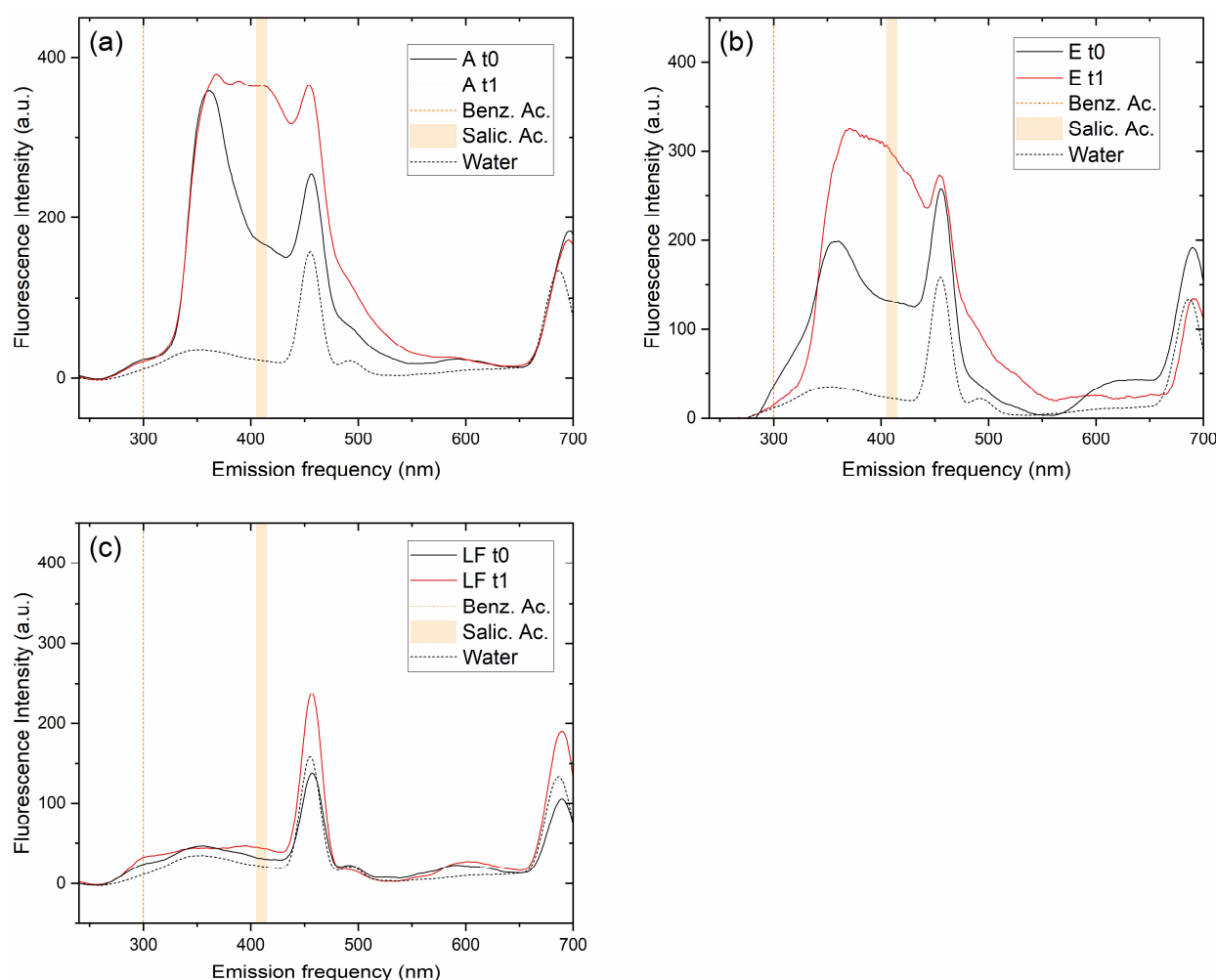


Figure 4. Fluorescence spectral patterns against UV irradiation time ($t_1 = 1$ h) in the decomposition of benzoic acid in the presence of (a) sample A (TiO_2), (b) sample E, and (c) sample F (LaFeO_3). The excitation wavelength was 230 nm. Experimental conditions: 0.120 g L^{-1} catalyst loading, $[\text{BA}] = 1 \times 10^{-4} \text{ M}$, $\lambda = 380\text{--}800 \text{ nm}$ radiation. The measured solutions were obtained from the supernatant after centrifugation of the corresponding suspensions containing the photocatalyst. The peaks at ca. 460 nm and 690 nm are instrumental background, as evidenced by the spectrum of pure water excited in the same conditions, which is reported in each panel (\cdots line) to guide the eye. The expected location of the signals from benzoic and salicylic acids is indicated by yellow lines.

To assess the generality of the enhanced activity of the $\text{LaFeO}_3/\text{TiO}_2$ catalysts, the degradation of another aromatic carboxylic acid compound, namely 4-methoxycinnamic

acid (MCA), was studied under previous experimental conditions. MCA undergoes to rapid and reversible trans-cis photoisomerization under UV radiation [30]. As shown in Figure S4, up to 98% of MCA is degraded in the presence of composite catalysts after 120 min of irradiation, better than pure TiO_2 catalyst. To degrade 90% of the aromatic carboxylic acids the 6.2 wt% and 12.2 wt%- $\text{LaFeO}_3/\text{TiO}_2$ composites take <120 min in the case of MCA and 300 min for BA. Also, sample F shows a better performance with MCA substrate (72% in 120 min) as compared to BA (<10% in 300 min). As expected, the degradation of MCA is much faster than that of BA due to different degradation mechanisms. It is well known that the principal degradation pathway for cinnamic acid involves attack at the alkene group by a super oxide radical, generating benzaldehyde as the main intermediate. Benzaldehyde undergoes attack by hydroxyl radicals, generating OH substituted intermediates that are quickly decomposed to CO_2 [31].

2.3. Benzoic Acid Degradation Under 450 nm Light in $\text{LaFeO}_3/\text{TiO}_2$ Water Suspensions With and Without H_2O_2

The photocatalytic degradation of BA under monochromatic 450 nm light over different catalysts, with and without H_2O_2 , was evaluated, and the results are shown in Figure 5. The results evidence that without H_2O_2 the bare photocatalysts and all $\text{LaFeO}_3/\text{TiO}_2$ composites degraded less than 10% of BA (Figure 5a). As shown in Table 1, Garcia-Muñoz et al. also reported a far smaller activity of the composite photocatalysts under >420 nm when compared to the reactions performed under solar light [19]. On the contrary, tests with dyes show high photocatalytic activity of $\text{LaFeO}_3/\text{TiO}_2$ composites under visible light [14]. However, tests with dyes (or with any substrate absorbing radiation) do not distinguish between a pure photocatalytic process and a dye-sensitized one, the latter being dye-specific and not general [32]. This could be the reason why pure LaFeO_3 and $\text{LaFeO}_3/\text{TiO}_2$ composites, while demonstrated to work well in previous studies using dyes, were actually poorly effective without H_2O_2 , as shown in the present work.

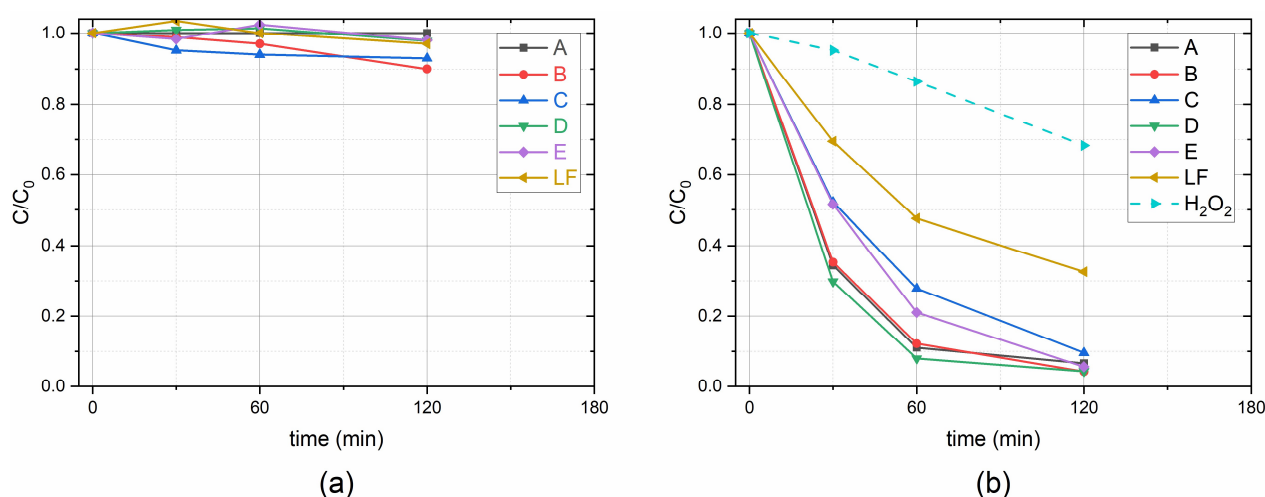


Figure 5. Photocatalytic degradation of BA in the presence of samples A (TiO_2), B (1.3 wt%- $\text{LaFeO}_3/\text{TiO}_2$), C (3.9 wt%- $\text{LaFeO}_3/\text{TiO}_2$), D (6.2 wt%- $\text{LaFeO}_3/\text{TiO}_2$), E (12.2 wt%- $\text{LaFeO}_3/\text{TiO}_2$) and LF (LaFeO_3), without H_2O_2 (a) and with H_2O_2 (b). Data from HPLC analysis. Experimental conditions: 0.120 g L^{-1} catalyst loading, $[\text{BA}] = 1 \times 10^{-4} \text{ M}$, $[\text{H}_2\text{O}_2] = 1 \text{ mM}$, under monochromatic 450 nm light. For reference, the degradation of BA in the presence of H_2O_2 without catalyst is shown (blue dotted line).

In the presence of H_2O_2 (1 mM), photocatalytic activity was high, and the most efficient samples were D, B and A. The pseudo-first-order rate constants (k) for BA degradation were determined for the initial reaction period (<120 min) and the values are reported in

Table 2. The D composite shows the highest reaction rate constant ($4.8 \times 10^{-4} \text{ s}^{-1}$), which is 1.2 and 3.2 times faster than those of TiO_2 ($4.1 \times 10^{-4} \text{ s}^{-1}$) and LaFeO_3 ($1.5 \times 10^{-4} \text{ s}^{-1}$), respectively. The radical intermediate HO^\bullet formed from H_2O_2 by reaction with the photogenerated electrons can act as an electron scavenger, thus inhibiting the e^- - h^+ pairs recombination at the semiconductor surface [33] according to the following equation:



where e_{CB}^- indicates electron excited to the conduction band.

Table 2. Values of the rate constant (k) for benzoic acid, and correlation coefficients of the linear fittings of the experimental data according to the pseudo-first-order reaction kinetic. Experimental conditions: 0.120 g L^{-1} catalyst loading, $[\text{BA}] = 1 \times 10^{-4} \text{ M}$, $[\text{H}_2\text{O}_2] = 1 \text{ mM}$, monochromatic 450 nm light.

Catalyst	$k \text{ (s}^{-1}\text{)}$	R^2
A	4.1×10^{-4}	0.934
B	4.4×10^{-4}	0.969
C	3.2×10^{-4}	0.996
D	4.8×10^{-4}	0.943
E	4.0×10^{-4}	0.995
F	1.5×10^{-4}	0.967

To further the study of the scarce activity of all photocatalysts without H_2O_2 under 450 nm light, degradation runs of 22 h were carried out. The results indicate that depending on composition, 30–60% of BA is degraded by the $\text{LaFeO}_3/\text{TiO}_2$ nanocomposites.

2.4. Hydrogen Evolution

Preliminary tests were performed by comparing the hydrogen evolution rate (HER) under UV-visible light radiation in the presence of pure TiO_2 (P25), pure LaFeO_3 and the composite materials B (1.3 wt%- $\text{LaFeO}_3/\text{TiO}_2$), C (3.9 wt%- $\text{LaFeO}_3/\text{TiO}_2$), D (6.2 wt%- $\text{LaFeO}_3/\text{TiO}_2$) and E (12.2 wt%- $\text{LaFeO}_3/\text{TiO}_2$), prepared by manual mixing of the two powders. Specifically, no hydrogen generation was observed in the presence of pure LaFeO_3 , due to the unsuitable band position of this photocatalyst (see Section 2.5), while the hydrogen amount was increased by 25% in the presence of the composite material when 1%wt. of LaFeO_3 was used. Based on these results, it was chosen to evaluate the effect of LaFeO_3 on HER, in the presence of methanol as the sacrificial agent.

As indicated in Figure 6, the hydrogen production rate follows a classical volcano-like behavior, with the highest reactivity in the presence of 3.86%wt of LaFeO_3 (sample C). Beyond this value, the reduction of HER can be probably be ascribed to the excessive coverage of titanium dioxide.

Furthermore, these materials were tested to assess the photocatalytic activity under visible light radiation. In this case, no hydrogen generation was observed probably due to (i) the wide band gap of titanium dioxide, as well as (ii) the unsuitable band gap position of LaFeO_3 (see the next section). Some experiments were conducted to assess how the system's temperature impacts photocatalytic hydrogen production. Indeed, temperature does not directly affect the photocatalytic process, as it primarily depends on the radiation wavelength and the material's absorption properties. However, the system's temperature may influence photocatalytic hydrogen generation by altering the adsorption behavior of organic species on the catalyst surface and modifying the reaction kinetics [34]. As illustrated in Figure 7, the amount of hydrogen produced increases as the system's temperature

risks with a HER 4.5-fold higher at the maximum tested temperature (i.e., 60 °C), with respect to the lowest temperature (i.e., 25 °C).

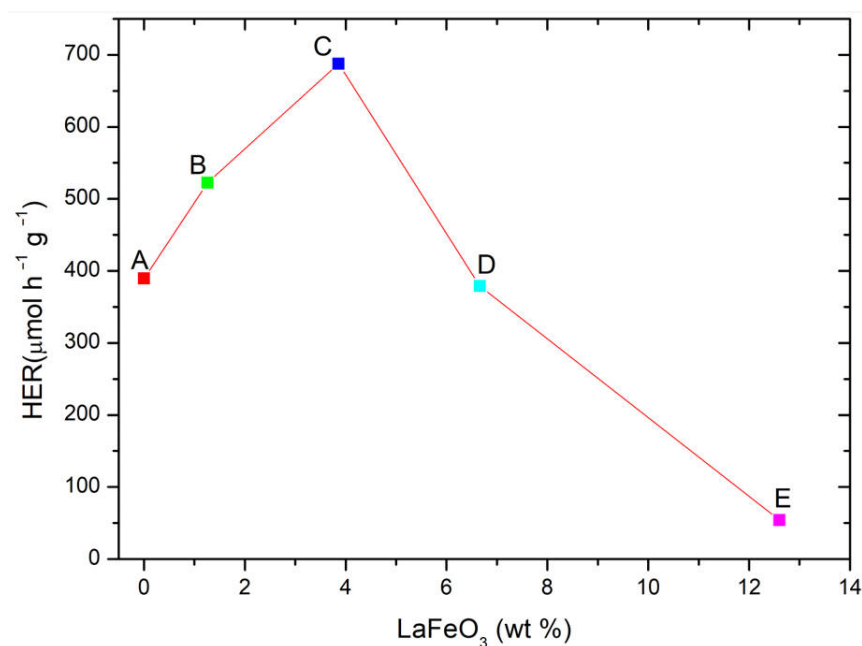


Figure 6. Photocatalytic hydrogen evolution rate (HER) at varying LaFeO₃ (%wt.) with respect to P25. Methanol was used as a model scavenger. Experimental conditions: [Methanol] = 2.5 M; 0.5 g L⁻¹ catalyst loading (Sample C); V = 0.3 L; T = 35 °C; natural pH of the solution.

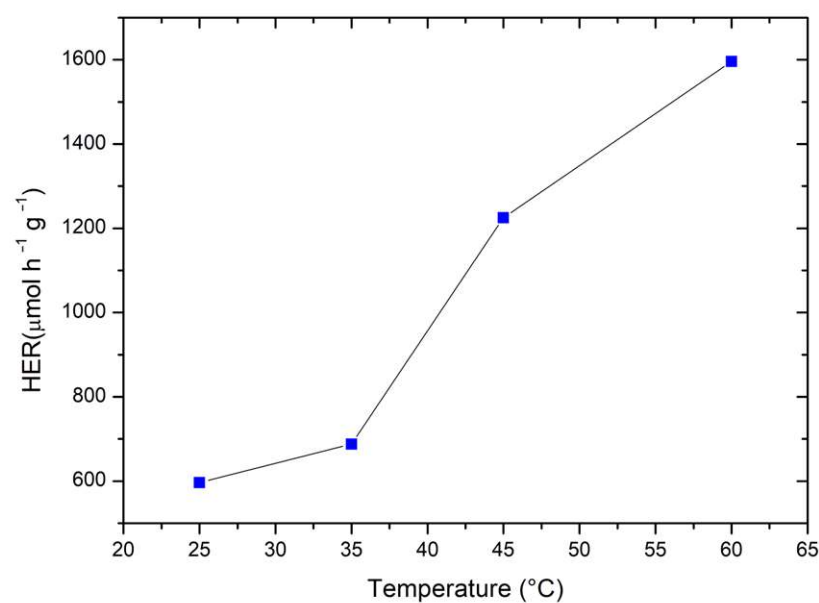


Figure 7. Photocatalytic hydrogen evolution rate (HER) at varying temperature of the system. Methanol was used as a model scavenger. Experimental conditions: [Methanol] = 2.5 M; 0.50 g L⁻¹ catalyst loading (Sample C); V = 0.3 L; natural pH of the solution.

Finally, photostability and reusability tests (Figure 8A,B) demonstrated good photostability both (i) during a single experiment carried out up to 8 h of irradiation, and (ii) during 4 photocatalytic cycles.

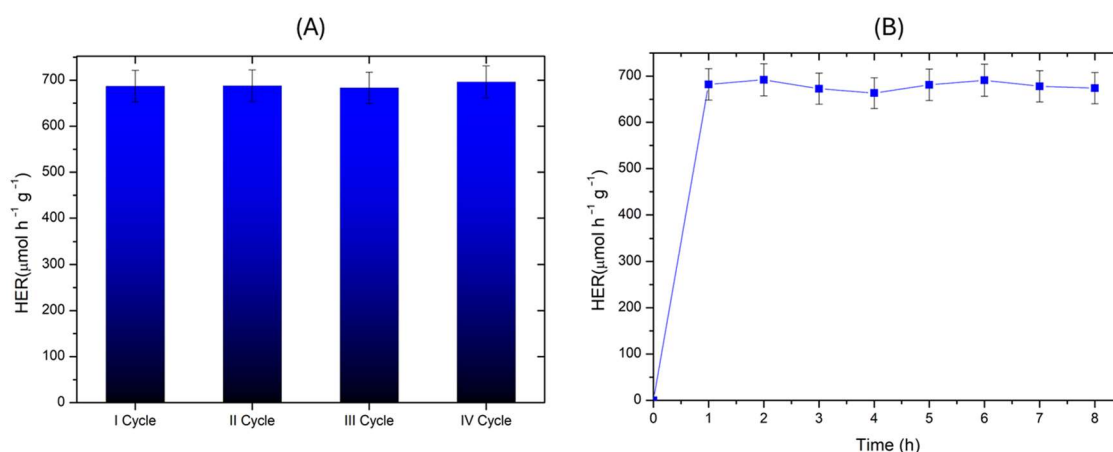


Figure 8. (A) Photocatalytic hydrogen evolution rate (HER) in successive photocatalytic tests. (B) Photocatalytic hydrogen evolution rate (HER) during a single photostability test. Methanol was used as a model scavenger. Experimental conditions: [Methanol] = 2.5 M; 0.50 g L^{-1} catalyst loading (Sample C); $V = 0.3 \text{ L}$; natural pH of the solution; $T = 35^\circ \text{C}$.

2.5. Activation of $\text{LaFeO}_3/\text{TiO}_2$ Nanocomposites

Different types of photogenerated charge-carrier transfer mechanism have been proposed for $\text{LaFeO}_3/\text{TiO}_2$ composites: type-II double charge transfer mechanism [14], direct Z-scheme mechanism [23], S-scheme [20], and uncommon heterojunction [16]. The formation of a p–n heterojunction between TiO_2 (n-type semiconductor) and LaFeO_3 (p-type semiconductor) could avoid e^-h^+ recombination and improve the activity. The valence band potential of a semiconductor at the point of zero charge can be calculated by the following empirical equation:

$$E_{\text{VB}} = X - E^e + 0.5E_{\text{g}} \quad (2)$$

where E_{VB} is the VB edge potential, X is the electronegativity of the semiconductor, which is the geometric mean of the electronegativity of the constituent atoms, E^e is the energy of free electrons on the hydrogen scale (about 4.5 eV), and E_{g} is the band gap energy of the semiconductor [35]. The conduction band potential E_{CB} can be determined by the equation $E_{\text{CB}} = E_{\text{VB}} - E_{\text{g}}$. The X values for LaFeO_3 and TiO_2 (anatase) are about 5.57 and 5.78 eV, respectively. The calculated E_{CB} and E_{VB} edge potentials for LaFeO_3 are +0.1 eV and +2.3 eV vs. SHE, as shown in Figure 9. For TiO_2 , E_{CB} and E_{VB} are -0.3 eV and $+2.9 \text{ eV}$ vs. SHE, in agreement with previous studies [17,20]. Before contact between the semiconductors, the calculated E_{VB} of LaFeO_3 is under that of the TiO_2 and E_{CB} is above that of the TiO_2 . The creation of a p–n heterojunction would modify the electronic band structure of both semiconductors. Since composites do not have significant photocatalytic activity under visible light in these samples, p–n heterojunction formation is quite unlikely, so a high rate of recombination of photogenerated charge is present.

In our study, the influence of the LaFeO_3 content was as follows: (i) under pure visible light better results are achieved by samples with a lower amount of LaFeO_3 (B and C); (ii) under visible light and a fraction of UV-A radiation, samples with higher wt% of LaFeO_3 (D and E) are more active; (iii) finally, the composites analyzed were not able at all to produce hydrogen under visible light. This behavior can suggest different light-mediated reaction mechanisms depending on the light wavelengths. Also, Garcia-Muñoz et al. reported the influence of the LaFeO_3 content on degradation of myclobutanil, but the optimum was observed at 5 wt% under solar light and 12.5 wt% under visible light, respectively [19]. The different behavior it is probably related to the core-shell system study by Garcia-Muñoz et al., while our composites are physical mixtures of the two components where TiO_2 particles are well dispersed on LaFeO_3 agglomerates.

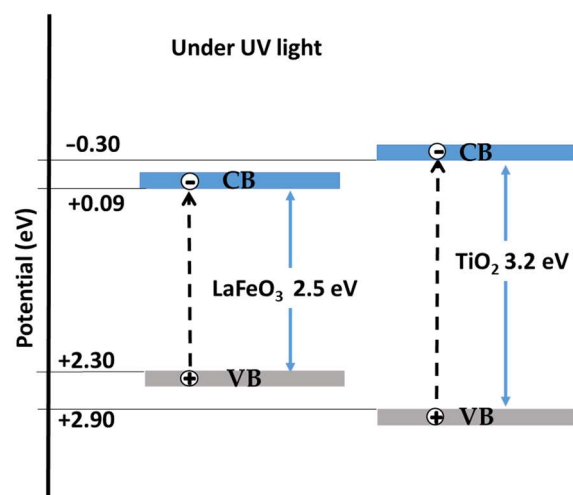


Figure 9. Scheme of the energy band structures and the correspondingly transfer process of photo-generated electron–hole pairs of semiconductor photocatalysts under UV light.

3. Materials and Methods

3.1. Chemicals and Preparations

Reactants for synthesis and chemicals for the photocatalytic reactions were purchased from Sigma-Aldrich (Saint Louis, MO, USA): La_2O_3 , $\text{Fe}(\text{NO}_3)_3 \cdot 9\text{H}_2\text{O}$, citric acid hydrate ($\text{C}_6\text{H}_8\text{O}_7 \cdot x\text{H}_2\text{O}$, 99.5%), H_2O_2 (>30%), nitric acid and NH_3 (30% aqueous solution). Lanthanum ferrite LaFeO_3 nanopowders were prepared using the citrate auto-combustion method. A specific amount of dried La_2O_3 was dissolved in a nitric acid solution to prepare $\text{La}(\text{NO}_3)_3 \cdot 6\text{H}_2\text{O}$. Stoichiometric amounts of metal nitrates were dissolved in water (0.1 mol L^{-1}) by stirring on a hotplate. The solution was poured in citric acid solution (molar ratio of metal ions to citric was 1:1). Aqueous NH_3 was added until the pH was 6.8. The solution was then dehydrated until a brown/orange gel formed. Dry gel was heated in air to 250°C to start ignition. The powder was then calcined at 600°C (5°C min^{-1}) in air for 3 h to decompose ammonium nitrate residues. A fast and simple procedure was employed to prepare the $\text{LaFeO}_3/\text{TiO}_2$ photocatalysts [36]. The method involved manual mixing of fixed quantities of TiO_2 (P25, nanopowder, mean particle diameter <50 nm, Sigma Aldrich) and LaFeO_3 in a vial. The wt% of LaFeO_3 to TiO_2 was 0 (sample A), 1.3 (sample B), 3.9 (sample C), 6.2 (sample D), 12.2 (sample E), and 100 (sample F) wt%. Then, a ball-milling method with an agate mortar and agate balls in a planetary mill was applied (PM100, RETSCH, Haan, Germany). The rotational speed (rpm) and milling time (min) were fixed at 1 min and 200 rpm, based on the previous studies on similar systems.

3.2. Microstructural Characterization

The powder X-ray diffraction patterns of the catalysts were recorded using a Bruker (Milano, Italy) D8-Advance powder diffractometer equipped with a $\text{Cu K}\alpha$ X-ray source and a Lynxeye XE-T[®] solid-state detector. The patterns were recorded in an interval of $10\text{--}90^\circ 2\theta$ with a step of 0.01° and a counting time of 1 s per step. Brunauer–Emmett–Teller (BET) specific surface area (SSA) determination was performed with nitrogen absorption on about 500 mg of the samples using a Micrometric (Norcross, GA, USA) Tristar 3000 automated gas-adsorption analyzer.

Scanning electron microscopy (SEM) was performed using a FEI (Hillsboro, OR, USA) Quanta 200 ESEM microscope, operating at 20 kV on specimens from which a thin layer of gold had evaporated. On the other hand, an electron microprobe used in an energy dispersive mode (EDX) was employed to obtain information on the actual metal–content ratio present in the samples. The UV-Vis diffuse reflectance spectroscopy (DRS) spectrum

of LaFeO₃ powder was recorded in the 200–800 nm range by using a Jasco (Tokyo, Japan) V-650 spectrophotometer equipped with an integrating sphere for solid samples, with BaSO₄ as the reference sample. The plot of the Kubelka–Munk function $(F(R_{\infty}) \times E)^2$ vs. photon energy (E) suggests a direct bandgap transition of 2.47 eV for LaFeO₃.

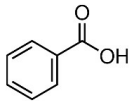
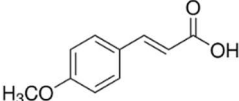
3.3. Florescence Spectroscopy

The fluorescence spectra reported in this work were recorded with a JASCO FP 6600 spectrofluorometer selecting the excitation wavelength of 230 nm, which corresponds to the experimental condition used to investigate photodegradation phenomena in benzoic/salicylic acids (Hidaka et al., 2006 [29]). The sample was placed in a Suprasil® quartz cuvette and the emission signal was collected at 90° to the excitation beam.

3.4. Photocatalytic Studies

The photocatalytic activity was evaluated by the degradation of benzoic acid (BA) and 4-methoxycinnamic acid (MCA); their main characteristics are shown in Table 3. The tests were performed under UV (LED lamp, 365 nm) and visible light irradiation (LED lamp, 450 nm Penn Photoreactor M2 and Multiray Daylight/fluorescent 380–800 nm). In a typical test, 2.4 mg of photocatalyst powder was added to 20 mL of a 1.1×10^{-4} M (13.4 mg L⁻¹) aqueous solution of BA. Before turning on the light, the mixture was stirred in the dark for 20 min in a 40 mL vial in order to allow adsorption/desorption equilibrium on the catalyst surface. At different time intervals (0 ÷ 5 h), aliquots of the reacting suspension (2.6 mL) were collected. The samples were centrifugated for 10 min at 450 rpm and the supernatants were analyzed with a UV-Vis spectrophotometry and high-pressure liquid chromatography, HPLC (Agilent 1200 series, CA, USA, column Zorbax Eclipse XDB-C18 4.6 × 150 mm, λ 228 nm, eluent water/methanol 6:4 + 1.5% acetic acid). The catalytic activity of the composites was evaluated with and without hydrogen peroxide addition (1 mM).

Table 3. Main physical–chemical properties of benzoic acid and 4-methoxycinnamic acid.

	Benzoic Acid	4-Methoxycinnamic Acid
N. CAS	65-85-0	943-89-5
Chemical structure		
Molecular formula	C ₆ H ₅ COOH	C ₁₀ H ₁₀ O ₃
Molecular mass	122.12 g/mol	178.18 g/mol
Physical form	White powder	White powder
Solubility in water	3.4 g/L at 25 °C	0.71 g/L at 25 °C
pKa	4.19	4.60

A 0.3 L glass batch reactor was employed for the photocatalytic hydrogen evolution experiments, equipped with a medium-pressure mercury lamp (Nominal Power P = 125 W) and a thermostat to control the temperature of the system. At a fixed temperature (25 °C ÷ 60 °C), during a typical experiment, a selected amount of photocatalyst (500 ppm) was suspended in a methanol aqueous solution (2.5 M). To prevent the reaction between dissolved oxygen and the photogenerated electrons, a nitrogen (N₂) stream was bubbled into the solution starting 40 min before the experiment. A Gas Chromatograph (Agilent 7820A) with an HP-PLOT Molesieve 5A column (Agilent) and a TCD detector, with argon as the carrier gas was utilized for the estimation of hydrogen production.

4. Conclusions

We have developed a facile and cost-effective approach to the preparation of a LaFeO₃/TiO₂ (P25) composites with LaFeO₃ wt% up to 12.2%. SEM analysis of the composites evidenced that the agglomerates of LaFeO₃ have an average size in the 1 to 5 µm range and the TiO₂ powder is well dispersed onto the surface of each sample. This characteristic seems to have some relationship with their good performance on the photocatalytic degradation of benzoic acid. The composites display enhanced photocatalytic activity when 380–800 nm light is used for irradiation; for example, 6.2 wt% and 12.2 wt%-LaFeO₃/TiO₂ composites degrade 93% of BA in 300 min compared to 80% for TiO₂. Fluorescence measurements corroborated that salicylic acid is one of the intermediates formed during the degradation of BA by OH• radical attack. Under 450 nm LED light, all LaFeO₃/TiO₂ composites degraded less than 10% of BA, but in the presence of H₂O₂ (1 mM) the photocatalytic activity was as high as 96% in <120 min, 6.2 wt%-LaFeO₃/TiO₂ composite being the most efficient sample. Then, the catalysts were suspended in a methanol aqueous solution (2.5 M) and irradiated under UV-visible light. A hydrogen evolution rate of 700 µmol h^{−1} g^{−1} was measured for the 3.86%wt-LaFeO₃/TiO₂ nanocomposite and good recyclability was established. The photocatalytic activity of LaFeO₃/TiO₂ composites is characterized by a volcano-like profile for both the BA degradation and the hydrogen evolution, but the optimum semiconductors ratio (LaFeO₃:TiO₂) depends on the wavelength of activating light. The mechanism of the photocatalytic degradation is proposed to involve the photoactivation of both LaFeO₃ and TiO₂ phases, leading to the formation of photogenerated charges (e^- - h^+) in both semiconductors. Further, the improvement of the photoactivity of the composites can be attributed to their larger surface area compared to pure LaFeO₃ and good dispersion of TiO₂ over the surface of LaFeO₃, which might have decreased the recombination center.

Supplementary Materials: The following supporting information can be downloaded at <https://www.mdpi.com/article/10.3390/molecules30071526/s1>, Figure S1: SEM images of LaFeO₃ powder. Figure S2: SEM image and EDX spectrum of C sample. Figure S3: Plot of Kubelka-Munk function $(F(R_\infty)/E)^2$ vs. photon energy obtained from DRS for band gap calculation of LaFeO₃. Figure S4: Photocatalytic degradation of MCA up to 120 min of irradiation from UV-vis data. Experimental conditions: 0.120 g L^{−1} catalyst loading, [MCA] = 2.5×10^{-5} M under 380–800 nm light. For reference, the MCA photolysis is reported (red stars).

Author Contributions: Conceptualization, I.N.S., R.P. and M.M.; methodology, I.N.S., B.B., R.P., A.L., M.T. and M.M.; validation I.N.S., B.B., R.P., A.L., M.T. and M.M.; investigation, I.N.S., B.B., R.P., A.L., M.T. and M.M.; resources, I.N.S. and M.M.; data curation, R.P.; writing—original draft preparation, I.N.S. and M.M.; writing—review and editing, I.N.S., M.T. and M.M.; visualization, R.P.; supervision, I.N.S. and M.M. All authors have read and agreed to the published version of the manuscript.

Funding: This research received no external funding.

Institutional Review Board Statement: Not applicable.

Informed Consent Statement: Not applicable.

Data Availability Statement: The data presented in this study are available on request from the corresponding author.

Conflicts of Interest: The authors declare no conflicts of interest.

References

- Kumari, H.; Ranga, R.; Chahal, S.; Devi, S.; Sharma, S.; Kumar, S.; Kumar, P.; Kumar, S.; Kumar, A.; Parmar, R. A Review on Photocatalysis Used For Wastewater Treatment: Dye Degradation. *Water Air Soil Pollut.* **2023**, *234*, 349. [\[CrossRef\]](#) [\[PubMed\]](#)
- Wang, H.; Li, X.; Zhao, X.; Li, C.; Song, X.; Zhang, P.; Huo, P. A Review on Heterogeneous Photocatalysis for Environmental Remediation: From Semiconductors to Modification Strategies. *Chin. J. Catal.* **2022**, *43*, 178–214. [\[CrossRef\]](#)
- Karthikeyan, C.; Arunachalam, P.; Ramachandran, K.; Al-Mayouf, A.M.; Karuppuchamy, S. Recent Advances in Semiconductor Metal Oxides with Enhanced Methods for Solar Photocatalytic Applications. *J. Alloys Compd.* **2020**, *828*, 154281. [\[CrossRef\]](#)
- Low, J.; Yu, J.; Jaroniec, M.; Wageh, S.; Al-Ghamdi, A.A. Heterojunction Photocatalysts. *Adv. Mater.* **2017**, *29*, 1601694. [\[CrossRef\]](#)
- Gómez, L.D.; Rodríguez-Páez, J.E. Micro/Nanoscale Mesoporous Nb₂O₅ Particles: Effect of Synthesis Conditions and Doping with N, C, or S on Their Properties. *Nano-Struct. Nano-Objects* **2019**, *17*, 43–57. [\[CrossRef\]](#)
- Hoffmann, M.R.; Martin, S.T.; Choi, W.; Bahnemann, D.W. Environmental Applications of Semiconductor Photocatalysis. *Chem. Rev.* **1995**, *95*, 69–96. [\[CrossRef\]](#)
- Pelaez, M.; Nolan, N.T.; Pillai, S.C.; Seery, M.K.; Falaras, P.; Kontos, A.G.; Dunlop, P.S.M.; Hamilton, J.W.J.; Byrne, J.A.; O'Shea, K.; et al. A Review on the Visible Light Active Titanium Dioxide Photocatalysts for Environmental Applications. *Appl. Catal. B Environ.* **2012**, *125*, 331–349. [\[CrossRef\]](#)
- Ni, M.; Leung, M.K.H.; Leung, D.Y.C.; Sumathy, K. A Review and Recent Developments in Photocatalytic Water-Splitting Using TiO₂ for Hydrogen Production. *Renew. Sustain. Energy Rev.* **2007**, *11*, 401–425. [\[CrossRef\]](#)
- Henderson, M.A. A Surface Science Perspective on TiO₂ Photocatalysis. *Surf. Sci. Rep.* **2011**, *66*, 185–297. [\[CrossRef\]](#)
- Sora, I.N.; Fontana, F.; Passalacqua, R.; Ampelli, C.; Perathoner, S.; Centi, G.; Parrino, F.; Palmisano, L. Photoelectrochemical Properties of Doped Lanthanum Orthoferrites. *Electrochim. Acta* **2013**, *109*, 710–715. [\[CrossRef\]](#)
- Bolognino, I.; Pelosato, R.; Marci, G.; Natali Sora, I. Comparison of Ten Metal-Doped LaFeO₃ Samples on Photocatalytic Degradation of Antibiotics in Water under Visible Light: Role of Surface Area and Aqueous Phosphate Ions. *Molecules* **2023**, *28*, 3807. [\[CrossRef\]](#)
- Pelosato, R.; Carrara, V.; Sora, I.N. Enhanced Photocatalytic Degradation of Ibuprofen in Aqueous Solution under Visible-Light Irradiation: Effects of LaFeO₃ and Cu/LaFeO₃. *Chem. Eng. Trans.* **2019**, *73*, 181–186. [\[CrossRef\]](#)
- Turkten, N.; Sora, I.N.; Tomruk, A.; Bekbolet, M. Photocatalytic Degradation of Humic Acids Using LaFeO₃. *Catalysts* **2018**, *8*, 630. [\[CrossRef\]](#)
- Dhinesh Kumar, R.; Thangappan, R.; Jayavel, R. Synthesis and Characterization of LaFeO₃/TiO₂ Nanocomposites for Visible Light Photocatalytic Activity. *J. Phys. Chem. Solids* **2017**, *101*, 25–33. [\[CrossRef\]](#)
- Jing, L.; Qu, Y.; Su, H.; Yao, C.; Fu, H. Synthesis of High-Activity TiO₂-Based Photocatalysts by Compounding a Small Amount of Porous Nanosized LaFeO₃ and the Activity-Enhanced Mechanisms. *J. Phys. Chem. C* **2011**, *115*, 12375–12380. [\[CrossRef\]](#)
- Humayun, M.; Li, Z.; Sun, L.; Zhang, X.; Raziq, F.; Zada, A.; Qu, Y.; Jing, L. Coupling of Nanocrystalline Anatase TiO₂ to Porous Nanosized LaFeO₃ for Efficient Visible-Light Photocatalytic Degradation of Pollutants. *Nanomaterials* **2016**, *6*, 22. [\[CrossRef\]](#)
- Tashkandi, N.Y.; Albukhari, S.M.; Ismail, A.A. Visible-Light Driven of Heterostructured LaFeO₃/TiO₂ Photocatalysts for Degradation of Antibiotics: Ciprofloxacin as Case Study. *J. Photochem. Photobiol. A Chem.* **2022**, *432*, 114078. [\[CrossRef\]](#)
- Hao, P.; Shi, R.; Wang, X.; Zhang, J.; Li, B.; Wang, J.; Liu, B.; Liu, Y.; Qiao, X.; Wang, Z. Efficient Tetracycline Degradation Using Carbon Quantum Dot Modified TiO₂@LaFeO₃ Hollow Core Shell Photocatalysts. *Sci. Rep.* **2024**, *14*, 27057. [\[CrossRef\]](#)
- Garcia-Muñoz, P.; Fresno, F.; Ivanez, J.; Robert, D.; Keller, N. Activity Enhancement Pathways in LaFeO₃@TiO₂ Heterojunction Photocatalysts for Visible and Solar Light Driven Degradation of Myclobutanil Pesticide in Water. *J. Hazard. Mater.* **2020**, *400*, 123099. [\[CrossRef\]](#)
- Pandey, V.; Bansal, A.; Toor, A.P. Synthesis and Performance Evaluation of S-Scheme Heterostructured LaFeO₃/TiO₂ Photocatalyst for the Efficient Degradation of Thiamethoxam. *Environ. Sci. Pollut. Res.* **2024**, *31*, 28578–28593. [\[CrossRef\]](#)
- Dai, J.; Zhu, Y.; Tahini, H.A.; Lin, Q.; Chen, Y.; Guan, D.; Zhou, C.; Hu, Z.; Lin, H.-J.; Chan, T.-S.; et al. Single-Phase Perovskite Oxide with Super-Exchange Induced Atomic-Scale Synergistic Active Centers Enables Ultrafast Hydrogen Evolution. *Nat. Commun.* **2020**, *11*, 5657. [\[CrossRef\]](#) [\[PubMed\]](#)
- Yu, J.; Li, Z.; Liu, T.; Zhao, S.; Guan, D.; Chen, D.; Shao, Z.; Ni, M. Morphology Control and Electronic Tailoring of CoxAy (A = P, S, Se) Electrocatalysts for Water Splitting. *Chem. Eng. J.* **2023**, *460*, 141674. [\[CrossRef\]](#)
- Lv, T.; Wang, H.; Hong, W.; Wang, P.; Jia, L. In Situ Self-Assembly Synthesis of Sandwich-like TiO₂/Reduced Graphene Oxide/LaFeO₃ Z-Scheme Ternary Heterostructure towards Enhanced Photocatalytic Hydrogen Production. *Mol. Catal.* **2019**, *475*, 110497. [\[CrossRef\]](#)
- Jiang, Y.; Lv, Q.; Xu, F.; Sun, X.; Ding, Y. Synthesis of TiO₂/LaFeO₃ Composites for the Photoelectrochemical Hydrogen Evolution. *J. Mater. Sci.* **2021**, *56*, 15188–15204. [\[CrossRef\]](#)
- Li, K.; Wang, D.; Wu, F.; Xie, T.; Li, T. Surface Electronic States and Photovoltage Gas-Sensitive Characters of Nanocrystalline LaFeO₃. *Mater. Chem. Phys.* **2000**, *64*, 269–272. [\[CrossRef\]](#)
- Kosmulski, M. pH-Dependent Surface Charging and Points of Zero Charge II. Update. *J. Colloid Interface Sci.* **2004**, *275*, 214–224. [\[CrossRef\]](#) [\[PubMed\]](#)

27. Mrowetz, M.; Selli, E. Photocatalytic Degradation of Formic and Benzoic Acids and Hydrogen Peroxide Evolution in TiO₂ and ZnO Water Suspensions. *J. Photochem. Photobiol. A Chem.* **2006**, *180*, 15–22. [[CrossRef](#)]
28. Ajmera, A.A.; Sawant, S.B.; Pangarkar, V.G.; Beenackers, A.A.C.M. Solar-Assisted Photocatalytic Degradation of Benzoic Acid Using Titanium Dioxide as a Photocatalyst. *Chem. Eng. Technol.* **2002**, *25*, 173–180. [[CrossRef](#)]
29. Hidaka, H.; Honjo, H.; Horikoshi, S.; Serpone, N. Photocatalyzed Degradation on a TiO₂-Coated Quartz Crystal Microbalance. Adsorption/Desorption Processes in Real Time in the Degradation of Benzoic Acid and Salicylic Acid. *Catal. Commun.* **2006**, *7*, 331–335. [[CrossRef](#)]
30. Smith, G.J.; Miller, I.J. The Effect of Molecular Environment on the Photochemistry of P-Methoxycinnamic Acid and its Esters. *J. Photochem. Photobiol. A Chem.* **1998**, *118*, 93–97. [[CrossRef](#)]
31. Bouleghlimat, E.; Bethell, D.; Davies, P.R. The Photocatalytic Destruction of Cinnamic Acid and Cinnamyl Alcohol: Mechanism and the Effect of Aqueous Ions. *Chemosphere* **2020**, *251*, 126469. [[CrossRef](#)] [[PubMed](#)]
32. Barbero, N.; Vione, D. Why Dyes Should Not Be Used to Test the Photocatalytic Activity of Semiconductor Oxides. *Environ. Sci. Technol.* **2016**, *50*, 2130–2131. [[CrossRef](#)] [[PubMed](#)]
33. Grätzel, C.K.; Jirousek, M.; Grätzel, M. Decomposition of Organophosphorus Compounds on Photoactivated TiO₂ Surfaces. *J. Mol. Catal.* **1990**, *60*, 375–387. [[CrossRef](#)]
34. Muscetta, M.; Clarizia, L.; Race, M.; Andreozzi, R.; Marotta, R.; Di Somma, I. Visible—Light Driven Systems: Effect of the Parameters Affecting Hydrogen Production through Photoreforming of Organics in Presence of Cu₂O/TiO₂ Nanocomposite Photocatalyst. *Appl. Sci.* **2023**, *13*, 2337. [[CrossRef](#)]
35. Butler, M.A.; Ginley, D.S. Prediction of Flatband Potentials at Semiconductor-Electrolyte Interfaces from Atomic Electronegativities. *J. Electrochem. Soc.* **1978**, *125*, 228–232. [[CrossRef](#)]
36. Muscetta, M.; Jitan, S.A.; Palmisano, G.; Andreozzi, R.; Marotta, R.; Cimino, S.; Di Somma, I. Visible Light—Driven Photocatalytic Hydrogen Production Using Cu₂O/TiO₂ composites Prepared by Facile Mechanochemical Synthesis. *J. Environ. Chem. Eng.* **2022**, *10*, 107735. [[CrossRef](#)]

Disclaimer/Publisher’s Note: The statements, opinions and data contained in all publications are solely those of the individual author(s) and contributor(s) and not of MDPI and/or the editor(s). MDPI and/or the editor(s) disclaim responsibility for any injury to people or property resulting from any ideas, methods, instructions or products referred to in the content.